CHINESE OPTICS LETTERS

Vol. 19, No. 8 | August 2021

Tunable coherent perfect absorption in three-dimensional Dirac semimetal films

Jipeng Wu (伍计鹏)[1,2], Jie Tang (唐 杰)[1], Rongzhou Zeng (曾荣周)[2], Xiaoyu Dai (戴小玉)[3], and Yuanjiang Xiang (项元江)[1*]

[1] School of Physics and Electronics, Hunan University, Changsha 410082, China

[2] College of Traffic Engineering, Hunan University of Technology, Zhuzhou 412007, China

[3] College of Electrical and Information Engineering, Hunan University, Changsha 410082, China

*Corresponding author: xiangyuanjiang@126.com

Received December 14, 2020 | Accepted February 2, 2021 | Posted Online April 16, 2021

In this article, we investigate the phenomenon of coherent perfect absorption (CPA) with bulk Dirac semimetal (BDS) thin film. CPA of BDS appears at the frequency of 43.89 THz with 0° phase modulation of two coherent input lights. Meanwhile, it shows that CPA can be realized under oblique incidence circumstances for both TM and TE polarizations. Moreover, the frequency of CPA can be adjusted by altering the thickness of BDS thin film, and the dynamic regulation of CPA can be realized by changing the Fermi energy. Finally, the peak coherent absorption frequency can be controlled by changing the degeneracy factor.

Keywords: coherent perfect absorption; bulk Dirac semimetal; thin film; phase modulation.

DOI: 10.3788/COL202119.081601

1. Introduction

In the past several years, Dirac materials, for example, graphene and topological insulators, have received a lot of attention because of its excellent photoelectric characteristics[1–6]. They are widely used in optical storage, chemical and biological sensors, and optoelectronic devices[7,8]. With the development of Dirac materials, a perfect absorber based on Dirac materials has also received intense attention due to its potential applications in solar cells and photo detectors[9–11]. To achieve perfect absorption, various schemes have been proposed and designed. For example, Xiang *et al.* proved that perfect absorption can be realized in a critical coupling resonator formed by a graphene-based hyperbolic metamaterial and a dielectric Bragg reflector[12]. Guo *et al.* proposed a graphene-based waveguide composite structure to investigate enhanced and perfect absorption[13]. Wu *et al.* designed a composite structure of topological insulator and one-dimensional photonic crystal (1DPC) to discuss tunable and multichannel perfect absorption due to the excitation of optical Tamm states[14]. Although various absorbers have been designed to realize perfect absorption, it is difficult to control the absorption performance once the structure of the absorber is designed. It is desirable to manipulate the absorption performance without altering the intrinsic parameters of the structure; hence, we can add incident light at the other side of the structure.

When two coherent input beams illuminate the absorber, destructive interference exists between two input beams, leading to the phenomenon of perfect absorption. We call this phenomenon coherent perfect absorption (CPA). Thanks to the flexible tunability of the phase difference of two coherent input lights[15,16], it provides us an effective mean to regulate the coherent absorption performance. The phenomenon of CPA was firstly studied, to the best of our knowledge, in a simple silicon resonator[17]. Recently, different kinds of schemes have been designed to achieve CPA[18,19]. Particularly, the studies on CPA based on graphene emerge constantly due to its excellent optical characteristics. For instance, Fan *et al.* studied the phenomenon of tunable CPA in monolayer graphene and designed a coherent absorber formed by non-resonant two-dimensional (2D) carbon material graphene to achieve CPA[20,21]. Kakenov *et al.* reported that the electrically tunable CPA phenomenon can be realized by using a large-area graphene layer and a metallic reflective electrode spaced by an electrolytic medium[22]. However, graphene is a single-layer atomic material, resulting in its weak interaction with light. Moreover, the application of graphene is still restricted by the production of materials, and it may take several decades to develop the products relying on high purity graphene. These shortcomings limit the application and promotion of graphene in practical devices.

Bulk Dirac semimetal (BDS), treated as three-dimensional graphene, has attracted wide attention of industry and academia due to its excellent physical and chemical characteristics[23,24]. Similar to graphene, the most important optical property of

BDS is that the surface conductivity can be manipulated by flexibly altering the Fermi energy on the surface of BDS. However, compared to graphene, BDS thin film is relatively easy to manufacture, shows lower inherent loss, and has more stable physical characteristics. As a result, stable BDS has a greater application prospect than graphene in adjustable surface plasmon optical devices[25–27]. However, so far, few studies have been reported to realize the adjustable CPA phenomenon based on BDS.

In this article, the phenomenon of CPA based on BDS thin film has been studied. It is found that CPA of BDS appears at the frequency of 43.89 THz with 0° phase modulation of the two coherent input lights. Meanwhile, it shows that CPA can be realized under oblique incidence circumstances for both TM and TE polarizations. In addition, the frequency of CPA can be adjusted by altering the thickness of BDS thin film, and the dynamic regulation of CPA can be realized by changing the Fermi energy. Finally, the peak coherent absorption frequency can be controlled by changing the degeneracy factor. We firmly believe that this work can find practical applications in adjustable detections and signal modulations.

2. Methods

The designed coherent absorber is shown in Fig. 1, the BDS thin film with thickness of d is free-standing in vacuum, and two coherent beams (I_+ and I_-) illuminate on it with the same incident angle of θ. O_+ and O_- correspond to the output lights, and $t_\pm$ and $r_\pm$ are the transmission and reflection coefficients, respectively.

Generally, the surface conductivity of BDS can be described by the Kubo formula, written as the combination of inter-band and in-band processes. The conductivity is closely related to the radiation frequency ω, Fermi energy E_F, and environment temperature T. At the low-temperature limit $T \ll E_F$, the conductivity can be expressed as[24]

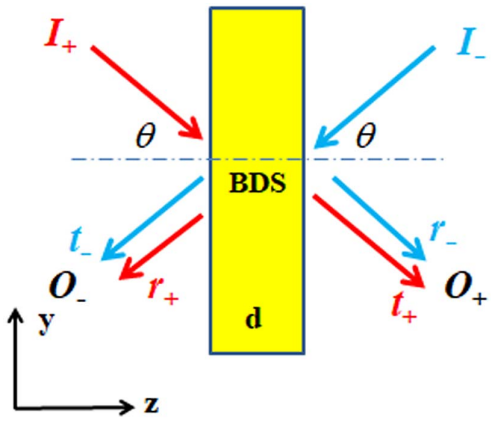

Fig. 1. Two coherent beams illuminate on the Dirac semimetal film, I_+ and I_- represent the coherent input beams, O_+ and O_- correspond to the output lights, the incident angle of the coherent input light is θ, and the thickness of the BDS film is d.

$$\mathrm{Re}\,\sigma(\Omega) = \frac{e^2}{\hbar}\frac{gk_F}{24\pi}\Omega\theta(\Omega-2), \tag{1}$$

$$\mathrm{Im}\,\sigma(\Omega) = \frac{e^2}{\hbar}\frac{gk_F}{24\pi^2}\left[\frac{4}{\Omega} - \Omega\ln\left(\frac{4\varepsilon_c^2}{|\Omega^2-4|}\right)\right], \tag{2}$$

where $\mathrm{Re}\,\sigma(\Omega)$ and $\mathrm{Im}\,\sigma(\Omega)$ represent the real and imaginary parts of conductivity, respectively, g is the degeneracy factor, $\hbar$ is the reduced Planck constant, e stands for the charge of a single electron, the Fermi momentum $k_F = E_F/(\hbar v_F)$, E_F expresses the Fermi energy, the Fermi velocity $v_F = 10^6$ m/s, $\Omega = \hbar\omega/E_F$, and $\varepsilon_c = E_c/E_F = 3$ (E_c is the cutoff energy). For further calculations, we should consider the Drude damping in Eqs. (1) and (2), and the expression of Ω is replaced by $\Omega \to \Omega + i\hbar\tau^{-1}/E_F$, where $\tau = 4.5\times10^{-13}$ s is the relaxation time. As a result, the relative permittivity of BDS can be expressed as a function of conductivity by a binary model[24]:

$$\varepsilon = \varepsilon_b + \frac{i\sigma}{\varepsilon_0\omega}, \tag{3}$$

where ε_0 is the permittivity of vacuum, and ε_b represents the effective permittivity of the medium, which relies on the value of g. For different values of g, we get the following constants ε_b: $\varepsilon_b = 1$ for $g = 40$ (AlCuFe quasi-crystals[28]), $\varepsilon_b = 6.2$ for $g = 24$ (Eu_2IrO_7[29] or TaAs family[30]), and $\varepsilon_b = 12$ for $g = 4$ (Na_3Bi[31] or Cd_3As_2[32,33]). According to the expression of surface conductivity and dielectric constant of BDS, it is known that we can manipulate the optical response of BDS by changing the Fermi energy E_F and the degeneracy factor g, and it will affect the coherent absorption of our structure. Therefore, in the following discussions, we focus on the influence of the Fermi energy and degeneracy factor on coherent absorption.

To describe the propagation of light in our designed structure, a transfer matrix can be used to calculate the transmission and reflection coefficients $t_\pm$ and $r_\pm$. The relationship between the output beams $O_\pm$ and the input beams $I_\pm$ can be linked by a scattering matrix, S, which can be described as

$$\begin{pmatrix} O_+ \\ O_- \end{pmatrix} = S\begin{pmatrix} I_+ \\ I_- \end{pmatrix} = \begin{pmatrix} t_+ & r_- \\ r_+ & t_- \end{pmatrix}\begin{pmatrix} Ae^{i\varphi_+} \\ Be^{i\varphi_-} \end{pmatrix}, \tag{4}$$

where $(r/t)_+$ and $(r/t)_-$ are scattering elements of forward I_+ and backward I_- lights. $A = |I_+|$ and $B = |I_-|$ are the amplitude of I_+ and I_-, and φ_+ and φ_- represent their phase, respectively. Considering the spatial and reciprocity symmetry of our designed structure, $t = t_\pm$ and $r = r_\pm$ can be used to simplify the scattering matrix. As a result, the coherent absorption A_C of our structure can be written as

$$A_C = 1 - (|t| - |r|)^2 - 2|tr|\left(1 + \cos\,\Delta\phi_1\,\cos\,\Delta\phi_2\frac{2AB}{A^2+B^2}\right), \tag{5}$$

where $\Delta\phi_1 = \mathrm{Arg}(t) - \mathrm{Arg}(r)$ represents the phase difference of the transmission and reflection coefficients, and $\Delta\phi_2 = \varphi_+ - \varphi_-$ stands for the phase difference between two input lights.

Considering a single beam incident on the BDS thin film, the structure can achieve total absorption only when the transmission and reflection coefficients are equal to zero. However, for such a structure, it is difficult to realize that the reflection and transmission coefficients are equal to zero simultaneously. Fortunately, for the coherent absorber, it is worthy of noting that the phenomenon of CPA appears when it meets conditions with $|t| = |r|$ and $1 + \cos\Delta\phi_1 \cos\Delta\phi_2 2AB/(A^2 + B^2) = 0$, which is $|t| = |r|$ and $A = B$. To simplify the discussion, we consider the amplitude of two coherent beams to be equal. This means that CPA is achieved in a reciprocal system by phase modulation, where the amplitudes of reflection and transmission coefficients are equal, and their phase difference is $n\pi$ with n being an arbitrary odd number.

3. Results and Discussions

To better understand the formation mechanism of CPA with BDS thin film, we plot the transmission and reflection coefficients with BDS thin film illuminated normally by a single input beam in Fig. 2. The relevant parameters are selected as $d = 3.1\,\mu m$, $E_F = 0.15\,eV$, and $g = 40$. Figure 2(a) exhibits the simulated spectra of transmission and reflection as functions of frequency. It is obvious that the transmission and reflection coefficients are equal at frequencies of 43.89 THz, 44.82 THz, 45.32 THz, and 45.55 THz, which shows potentiality for realizing the phenomenon of CPA. For achieving CPA, we further investigate the phase difference of reflection and transmission coefficients in Fig. 2(b). The phase difference is 180° at the frequency of 43.89 THz, which meets the condition of CPA. However, at three other frequencies, the phases of transmission and reflection coefficients are mismatched, and the phenomenon of CPA cannot be realized. The absorption of BDS thin film, $A_S = 1 - |r|^2 - |t|^2$, is also shown in Fig. 2(a). The absorption peak with the value of 55.5% appears at the frequency of 43.89 THz, meaning that the phenomenon of electromagnetic resonance occurs. Such a strong resonance makes it possible to realize CPA in our structure.

For further studying the formation process of CPA with BDS thin film, Fig. 3(a) plots coherent absorption as a function of frequency and phase difference of two coherent input beams. The perfect coherent absorption appears at the frequency of 43.89 THz, where the phase difference $\Delta\phi_2$ is zero (or $2n\pi$). At the frequency of 45.55 THz, there is another high absorption of 97% due to the small phase mismatch of the transmission and reflection coefficients. Figure 3(b) plots the coherent absorption with the change of phase difference $\Delta\phi_2$ at the frequency of 43.89 THz. The coherent absorption varies from 10.91% to 99.99% with the change of phase difference $\Delta\phi_2$, and the highest coherent absorption is obtained when the phase difference $\Delta\phi_2$ is 0°, which means that the phenomenon of CPA occurs.

In order to investigate the coherent absorption of our structure under oblique incidence circumstances, we plot the CPA frequency and the corresponding maximal coherent absorption at various incident angles for both TM-polarized

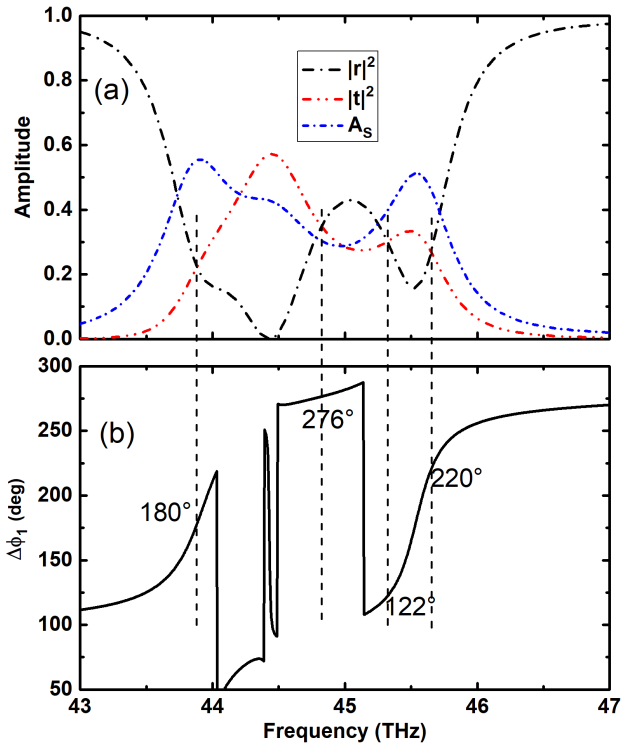

Fig. 2. (a) Spectra of transmission, reflection, and absorption for Dirac semimetal film illuminated normally by a single TM-polarized beam. (b) The corresponding phase difference of reflection and transmission coefficients.

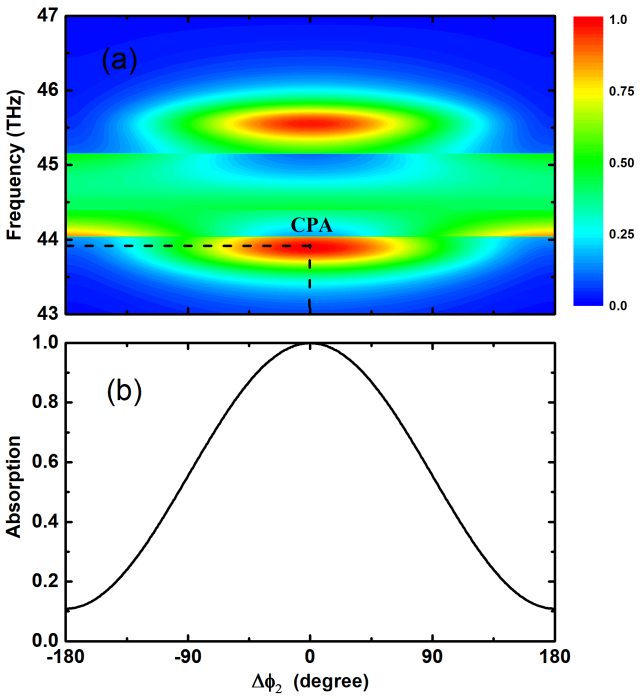

Fig. 3. (a) Coherent absorption as a function of frequency and phase difference of the two input beams, and the maximal coherent absorption appears at the frequency of 43.89 THz with zero phase difference. (b) The coherent absorption with the change of phase difference at the frequency of 43.89 THz.

and TE-polarized waves. As seen in Fig. 4(a), the frequency of CPA varies with the change of incident angle for both polarized waves. As the incident angle increases from 0° to 60°, the frequency of CPA has a blue shift from 43.89 THz to 46.39 THz for the TM-polarized wave, and the frequency of CPA changes fastest when the incident angle varies from 10° to 20°. However, as the incident angle varies from 60° to 70°, the frequency of CPA displays a fast red shift from 46.39 THz to 44.14 THz. For the TE-polarized wave, the frequency of CPA exhibits a blue shift with the incident angle increasing from 0° to 20° or 40° to 70°, and it has the maximum coherent absorption frequency at the incident angle of 30°. Figure 4(b) shows the corresponding maximal coherent absorption. The peak absorption for both polarizations reaches up to 96.8% at any incident angle. Particularly, for TM waves, as the incident angle varies from 0° to 10° or 30° to 70°, the coherent absorption keeps being higher than 99%, and for TE waves, as the incident angle varies from 0° to 30° or 60° to 70°, the coherent absorption also keeps being higher than 99%. Such characteristics give it more potential applications in optical switching and signal processing.

The thickness of BDS thin film influences the reflection and transmission coefficients of our structure, and it finally affects the formation of CPA. Figure 5 plots the coherent absorption as a function of frequency at different thicknesses of BDS thin film. The coherent absorption varies with the change of thickness. As the thickness increases from 3 μm to 3.2 μm, the peak

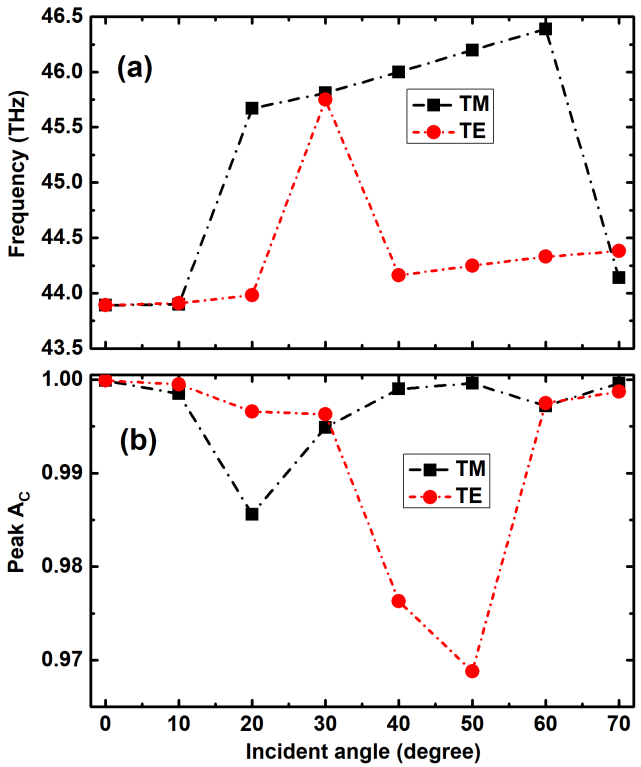

Fig. 4. (a) Frequency dispersion for TM-polarized and TE-polarized waves illuminating obliquely on the absorber and (b) the relevant maximal coherent absorption.

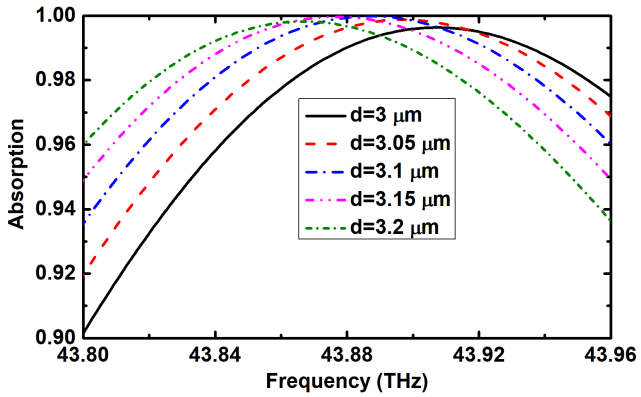

Fig. 5. Regulation of coherent absorption via changing the thickness of BDS thin film for the parameters E_F = 0.15 eV, g = 40, $\Delta\phi_2$ = 0, and θ = 0.

absorption frequency has a red shift from 43.91 THz to 43.87 THz. Moreover, the peak coherent absorption stays higher than 99% in all cases, meaning that nearly CPA can be realized at these different thicknesses. When the thickness increases from 3 μm to 3.1 μm, the corresponding maximum absorption peak exhibits an enhancement, while the maximum absorption peak decreases with the thickness varying from 3.1 μm to 3.2 μm. As a result, the thickness of 3.1 μm is the optimal thickness to achieve CPA.

Similar to graphene, the Fermi energy on the surface of BDS is an important influence on the surface conductivity of BDS, and the Fermi energy can be flexibly changed via electrostatic biasing. As a result, it provides us with an effective means to regulate coherent absorption of our structure. Figure 6 shows the manipulation of coherent absorption by altering the Fermi energy. The Fermi energy is chosen as 0.13 eV, 0.14 eV, 0.15 eV, 0.16 eV, and 0.17 eV. With the increase of Fermi energy, the absorption curves have a blue shift. When the Fermi energy changes from 0.13 eV to 0.16 eV, the peak coherent absorption stays higher than 99%, and, even if the Fermi energy is 0.17 eV, the peak coherent absorption is also greater than 96.7%, which means that nearly CPA can be realized in all cases. Therefore, the

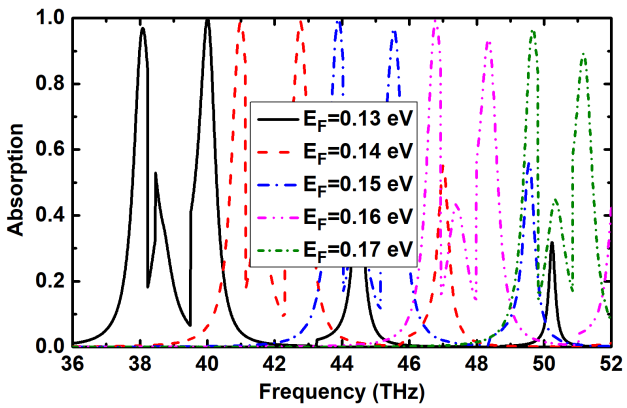

Fig. 6. Manipulation of coherent absorption by changing the Fermi energy E_F for the parameters g = 40, d = 3.1 μm, $\Delta\phi_2$ = 0, and θ = 0.

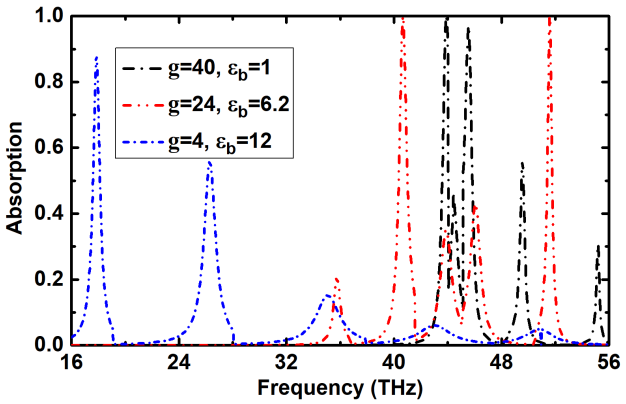

Fig. 7. Coherent absorption spectrum as a function of frequency for different degeneracy factors g, in which g = 40, ε_b = 1 corresponds to AlCuFe quasicrystals, g = 24, ε_b = 6.2 corresponds to Eu_2IrO_7, and g = 4, ε_b = 12 corresponds to Na_3Bi.

phenomenon of CPA at different frequencies can be easily achieved by simply changing the Fermi energy.

In addition to the above discussions, the degeneracy factor also affects the optical response of BDS. Figure 7 shows the coherent absorption as a function of frequency at different degeneracy factors. The degeneracy factors are chosen as 40, 24, and 4, which correspond to AlCuFe, Eu_2IrO_7, and Na_3Bi, respectively. The coherent absorption curve varies with the change of degeneracy factor. When the degeneracy factors are 40 or 24, the peak coherent absorption is as high as 99.9%, which means that CPA can be realized at these two different degeneracy factors. While the degeneracy factor is four, the peak coherent absorption declines to 87.8%, and the phenomenon of CPA disappears. As a result, the phenomenon of CPA at different frequencies can be achieved by choosing the appropriate degeneracy factor with other parameters of the structure fixed.

4. Conclusion

In conclusion, we have studied the phenomenon of CPA with BDS thin film. CPA of BDS can be realized in a reciprocal system by phase modulation of the two coherent input lights, where the amplitudes of transmission and reflection coefficients are equal by deriving the expression of coherent absorption. We demonstrate that the phenomenon of CPA appears at the frequency of 43.89 THz with 0° phase modulation of the two coherent input beams. Meanwhile, it exhibits that CPA can be realized under oblique incidence circumstances for both TM and TE polarizations. In addition, the frequency of CPA can be adjusted by changing the thickness of BDS thin film. More importantly, the Fermi energy can be changed via electrostatic biasing, so that the dynamic regulation of CPA can be realized. Finally, the peak coherent absorption frequency can be controlled by changing the degeneracy factor. We firmly believe that our work will show practical applications in adjustable detections and signal modulations.

Acknowledgement

This work was supported by the National Natural Science Foundation of China (Nos. 61875133 and 11874269), the Science and Technology Project of Shenzhen (Nos. JCYJ20190808143801672, JCYJ20190808150803580, JCYJ20180305125036005, JCYJ20180305124842330, and JCYJ20180305125443569), and the Natural Science Foundation of Guangdong (No. 2018A030313198).

References

1. T. Wenger, G. Viola, J. Kinaret, M. Fogelstrom, and P. Tassin, "Current-controlled light scattering and asymmetric plasmon propagation in graphene," Phys. Rev. B **97**, 085419 (2017).
2. I. Lee, D. Yoo, P. Avouris, T. Low, and S. Oh, "Graphene acoustic plasmon resonator for ultrasensitive infrared spectroscopy," Nat. Nanotech. **14**, 313 (2019).
3. A. Dankert, P. Bhaskar, D. Khokhriakov, I. Rodrigues, B. Karpiak, M. V. Kamalakar, S. Charpentier, I. Garate, and S. Dash, "Origin and evolution of surface spin current in topological insulators," Phys. Rev. B **97**, 125414 (2018).
4. M. Shiranzaei, J. Fransson, H. Cheraghchi, and F. Parhizgar, "Non-linear spin susceptibility in topological insulators," Phys. Rev. B **97**, 180402 (2018).
5. T. Jiang, R. Miao, J. Zhao, Z. Xu, T. Zhou, K. Wei, J. You, X. Zheng, Z. Wang, and X. Cheng, "Electron–phonon coupling in topological insulator Bi_2Se_3 thin films with different substrates," Chin. Opt. Lett. **17**, 020005 (2019).
6. L. Jiang, J. Tang, Q. Wang, Y. Wu, Z. Zheng, Y. Xiang, and X. Dai, "Manipulating optical Tamm state in the terahertz frequency range with graphene," Chin. Opt. Lett. **17**, 020008 (2019).
7. H. Yan, X. Li, B. Chandra, G. Tulevski, Y. Wu, M. Freitag, W. Zhu, P. Avouris, and F. Xia, "Tunable infrared plasmonic devices using graphene/insulator stacks," Nat. Nanotechnol. **7**, 330 (2012).
8. F. Bonaccorso, Z. Sun, T. Hasan, and A. C. Ferrari, "Graphene photonics and optoelectronics," Nat. Photon. **4**, 611 (2010).
9. J. Wu, L. Jiang, J. Guo, X. Dai, Y. Xiang, and S. Wen, "Turnable perfect absorption at infrared frequencies by a graphene-hBN hyper crystal," Opt. Express **24**, 17103 (2016).
10. Q. Yang, C. Zhang, S. Wu, S. Li, Q. Bao, V. Giannini, S. A. Maier, and X. Li, "Photonic surface waves enabled perfect infrared absorption by monolayer graphene," Nano Energy **48**, 161 (2018).
11. J. Hu, J. Fu, X. Liu, D. Ren, J. Zhao, and Y. Huang, "Perfect absorption in a monolayer graphene at the near-infrared using a compound waveguide grating by robust critical coupling," Chin. Opt. Lett. **17**, 010501 (2019).
12. Y. Xiang, X. Dai, J. Guo, H. Zhang, S. Wen, and D. Tang, "Critical coupling with graphene-based hyperbolic metamaterials," Sci. Rep. **4**, 5483 (2014).
13. J. Guo, L. Wu, X. Dai, Y. Xiang, and D. Fan, "Absorption enhancement and total absorption in a graphene-waveguide hybrid structure," AIP Adv. **7**, 025101 (2017).
14. J. Wu, Y. Liang, J. Guo, L. Jiang, X. Dai, and Y. Xiang, "Tunable and multichannel terahertz perfect absorber due to Tamm plasmons with topological insulators," Plasmonics **15**, 83 (2019).
15. G. Pirruccio, L. Martín Moreno, G. Lozano, and J. Gómez Rivas, "Coherent and broadband enhanced optical absorption in graphene," ACS Nano **7**, 4810 (2013).
16. Y. D. Chong, L. Ge, H. Cao, and A. D. Stone, "Coherent perfect absorbers: time-reversed lasers," Phys. Rev. Lett. **105**, 053901 (2010).
17. W. Wan, Y. Chong, L. Ge, H. Noh, A. D. Stone, and H. Cao, "Time-reversed lasing and interferometric control of absorption," Science **331**, 889 (2011).
18. W. R. Zhu, F. J. Xiao, M. Kang, and M. Premaratne, "Coherent perfect absorption in an all-dielectric metasurface," Appl. Phys. Lett. **108**, 121901 (2016).
19. L. Ying and A. Christos, "Tunable nonlinear coherent perfect absorption with epsilon-near-zero plasmonic waveguides," Opt. Lett. **43**, 983 (2018).
20. Y. Fan, F. Zhang, Q. Zhao, Z. Wei, and H. Li, "Tunable terahertz coherent perfect absorption in a monolayer graphene," Opt. Lett. **39**, 6269 (2014).

21. Y. Fan, Z. Liu, F. Zhang, Q. Zhao, Z. Wei, Q. Fu, J. Li, C. Gu, and H. Li, "Tunable mid-infrared coherent perfect absorption in a graphene meta-surface," Sci. Rep. **5**, 13956 (2015).
22. N. Kakenov, O. Balci, T. Takan, V. A. Ozkan, H. Altan, and C. Kocabas, "Observation of gate-tunable coherent perfect absorption of terahertz radiation in graphene," ACS Photon. **3**, 1531 (2016).
23. B. Rosenstein, B. Y. Shapiro, and I. Shapiro, "Collective modes, ac response, and magnetic properties of the three-dimensional Dirac semimetal in the triplet superconducting state," Phys. Rev. B **92**, S341 (2015).
24. O. V. Kotov and Y. E. Lozovik, "Dielectric response and novel electromagnetic modes in three-dimensional Dirac semimetal films," Phys. Rev. B **93**, 235417 (2016).
25. G. Liu, X. Zhai, H. Meng, L. Qi, H. Yu, C. Zhao, and L. Wang, "Dirac semimetals based tunable narrowband absorber at terahertz frequencies," Opt. Express **26**, 11471 (2018).
26. H. Xiong, Q. Shen, and Q. Ji, "Broadband dynamically tunable terahertz absorber based on Dirac semimetal," Appl. Opt. **59**, 4970 (2020).
27. K. Tang, Y. Su, M. Qin, X. Zhai, and L. Wang, "Dynamically tunable coherent perfect absorption and transparency in Dirac semimetal metasurface," Opt. Mater. Express **9**, 3649 (2019).
28. T. Timusk, J. P. Carbotte, C. C. Homes, D. N. Basov, and S. G. Sharapov, "Three-dimensional Dirac fermions in quasicrystals as seen via optical conductivity," Phys. Rev. B **87**, 235121 (2013).
29. A. B. Sushkov, J. B. Hofmann, G. S. Jenkins, J. Ishikawa, S. Makatsuji, S. D. Sarma, and H. D. Drew, "Optical evidence for a Weyl semimetal state in pyrochlore $Eu_2Ir_2O_7$," Phys. Rev. B **92**, 241108 (2015).
30. H. Weng, C. Fang, Z. Fang, B. A. Bernevig, and X. Dai, "Weyl semimetal phase in noncentrosymmetric transition-metal monophosphides," Phys. Rev. X **5**, 011029 (2014).
31. Z. K. Liu, B. Zhou, Y. Zhang, Z. J. Wang, H. M. Weng, D. Prabhakran, S. K. Mo, Z. X. Shen, Z. Fang, X. Dai, Z. Hussain, and Y. L. Chen, "Discovery of a three-dimensional topological Dirac semimetal, Na_3Bi," Science **343**, 864 (2014).
32. S. Borisenko, Q. Gibson, D. Evtushinsky, V. Zabolotnyy, B. Buchner, and R. J. Cava, "Experimental realization of a three-dimensional Dirac semimetal," Phys. Rev. Lett. **113**, 027603 (2013).
33. M. Neupane, S. Xu, R. Sankar, N. Alidoust, G. Bian, C. Liu, B. Ilya, T. R. Chang, H. T. Jeng, H. Lin, A. Bansil, F. Chou, and M. Z. Hasan, "Observation of a three-dimensional topological Dirac semimetal phase in high-mobility Cd_3As_2," Nat. Commun. **5**, 3786 (2013).